

Chapter 5

A Non-Oxidative Approach toward Chemically and Electrochemically Functionalizing

Si(111)

5.1 INTRODUCTION

Semiconductor devices and semiconductor processing are playing an increasingly large role in biotechnology applications. Examples include silicon nanowires (SiNWs)¹ and nanocantilevers^{2,3} for label-free biomolecular sensors, nanofluidics for biomolecular separations,⁴⁻⁷ and microfabricated lab-on-a-chip technologies.^{8,9} Coupled with these developments has been the emergence of mechanical,¹⁰⁻¹² chemical, and electrochemical approaches for functionalizing and/or selectively activating surfaces. For sensing applications, electrochemical activation of surfaces is particularly relevant since it is only limited by the size of electronically addressable features (which can be much denser than what can be spotted with an inkjet, for example). Electrochemical activation of metal surfaces has been pioneered by Mrksich and co-workers,¹³⁻¹⁶ and applications of that chemistry toward the spatially selective biofunctionalization of semiconductor nanowires has been demonstrated by at least two groups.^{17,18}

For silicon surfaces, the chemistry is particularly challenging because unprotected silicon forms a native oxide (SiO₂) layer. This native oxide layer can limit the use of silicon electrodes for electrochemical functionalization. Moreover, the native oxide on silicon has a low isoelectric point (~2). Therefore, SiO₂ surfaces are negatively charged under physiological conditions (= pH 7.4).¹⁹ These surface charges can potentially limit the sensitivity of SiNW field effect biosensors through Debye screening²⁰ by the localized ionic concentration at the sensor surface. Additionally, the native oxide layer contains electrical defect sites at the Si-SiO₂ interface.²¹ These electrical defect sites can detrimentally affect carrier recombination rates leading to decreased transistor or sensor performance in silicon-based nanoelectronic devices.²²

For high surface area devices, such as SiNWs, this phenomenon can reduce charge carrier mobilities significantly.²¹ Thus, the ideal biofunctionalization strategy for electrochemically activating silicon surfaces should begin with non-oxidized silicon. For sensing applications, the functionalization approach should provide continued protection of the silicon surface against further oxidation and limit the number of surface defect sites that can increase carrier recombination rates.

Several methods for attaching organic molecules onto non-oxidized silicon surfaces have been reported. One class of schemes relies on the direct covalent attachment of terminal alkenes on hydrogen-terminated surfaces by thermal induction, ultraviolet (UV) light, or catalysis.^{23–30} The resulting alkyl monolayers reflect the atomic flatness of the underlying silicon,^{31,32} and they provide partial chemical passivation of silicon via the formation of a Si-C bond. However, the alkyl monolayers prepared by the above strategies have not been demonstrated to give long-term protection to the silicon surface against oxidation due to limited molecular packing densities.

The Lewis group has developed techniques to alkylate chlorine-terminated Si(111) surfaces using alkylmagnesium and alkyllithium reagents.^{33–38} A limitation of these methods is that a 100% surface coverage can only be obtained with a methylated Si(111) surface, as confirmed by low-temperature STM.^{34,39} By comparison, the surface coverage achieved by the ethylation of chlorine-terminated Si(111) is limited by steric effects and corresponds to 80% of the atop silicon sites.⁴⁰ For more complex long-chain organic molecules, surface coverages will most certainly be lower, and the resistance to oxidation of the Si(111) surface will be reduced. It is therefore necessary to develop a surface chemistry method that will fully passivate the Si(111) surface, provide resistance

to oxide growth, and offer a chemical handle for the attachment of a variety of molecules. No methods have yet been demonstrated that protect the more technologically relevant Si(100) surface against oxidation.

This chapter describes the development of a versatile and robust strategy for chemically passivating Si(111) surfaces in a manner that stabilizes the underlying Si against native oxidation and allows for both chemical and electrochemical functionalization of the surface. Based on our previous work on methylated and ethylated Si(111),³³⁻⁴⁰ the more chemically versatile acetylenylation of chlorine-terminated Si(111) was explored. Work by Nemanick⁴¹ and Lewis' group^{42,43} indicated that the chlorination/alkylation chemistry for acetylenylating Si(111) could proceed to completion. The footprint of the linear *sp*-hybridized acetylene group (-C≡CH) on Si(111) should be as small or smaller than the -CH₃ group, and so a high surface coverage should be possible. Equally important is that the -C≡CH group also provides a chemical handle for additional functionalization via the Cu(I) catalyzed Huisgen 1,3-dipolar cycloaddition ('click' reaction^{44,45}) between an azide and the surface-bound alkyne. In particular, we designed an azide-functionalized, modified benzoquinone for attachment, via the click reaction, to the surface-bound acetylenyl groups to form a 1,2,3-triazole. The click reaction is useful because azides and acetylenes are synthetically easy to introduce, compatible with a variety of solvents and species, and tolerant against other functionalities (highly specific, coupling can only occur between these two groups). Our work here follows reports that have demonstrated that different molecules can be clicked onto gold and SiO₂ surfaces in a variety of solvent and pH conditions.⁴⁶⁻⁵⁴

We previously reported on the electrochemistry of hydroquinones on Si(111) and Si(100) surfaces, attached via the UV-activation of H-terminated Si.¹⁷ In that work, the hydroquinones could be reversibly oxidized to form benzoquinones (the ‘activated’ surface) which could then react by way of either Diels-Alder cycloaddition^{13,15} or Michael addition chemistries,^{55,56} leading to a selectively biofunctionalized silicon microwire or nanowire surface. However, while the hydroquinone coverage on the Si(111) surface did yield at least some protection for that surface against oxidation, the electrochemical step to oxidize the hydroquinone also led to oxidation of the underlying Si(111). Thus, in this work, we have designed and synthesized a benzoquinone that can be clicked onto the acetylenylated silicon surface. The surface-bound benzoquinone may be then activated via electrochemical *reduction* to produce an amine terminus.^{14,57,58} We demonstrate that the entire chemical process may be accomplished in a fashion that greatly reduces the oxidation of the underlying silicon. We also demonstrate the selective attachment of ferrocene onto an electrochemically activated Si(111) surface, as well as the model biomolecule, biotin.

5.2 MATERIALS AND EXPERIMENTAL METHODS

5.2.1 Chemicals

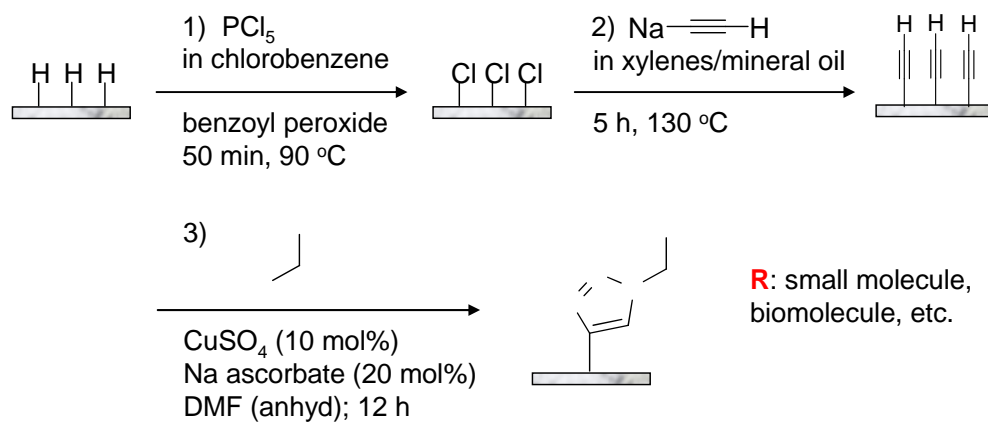
Anhydrous methanol and anhydrous tetrahydrofuran (THF, inhibitor-free) were obtained from Aldrich and exclusively stored and used in a N₂(g)-purged glove box. Chlorobenzene, benzoyl peroxide, and sodium acetylide (18 wt% in xylenes/light mineral oil) were purchased from Aldrich and were stored and used in the glove box. Phosphorus pentachloride (PCl₅) was acquired from Riedel-de Haën (Seelze, Germany). The 40% NH₄F(aq) solution was obtained from Transene Co. (Rowland, MA) and was

used as received. The $\text{CuSO}_4 \cdot 5\text{H}_2\text{O}$ was obtained from Spectrum Chemical Mfg. Corp. (Gardena, CA). Sodium ascorbate, ferrocene carboxylic acid, and anhydrous *N,N'*-dimethylformamide (DMF) were obtained from Aldrich. *N,N'*-Diisopropylcarbodiimide (DIC) was purchased from AnaSpec (San Jose, CA). Dulbecco's Phosphate Buffered Saline (DPBS) (2.7 mM KCl, 1.5 mM KH_2PO_4 , 137 mM NaCl, 8 mM Na_2HPO_4) pH 7.4 was purchased from Sigma. EZ-Link NHS-Biotin was obtained from Pierce Biotechnology (Rockford, IL). Nanogold Streptavidin was purchased from Invitrogen (Carlsbad, CA). GoldEnhance-EM kit for Nanogold amplification was bought from Nanoprobes (Yaphank, NY).

5.2.2 Acetylenylation of Si(111)

Scheme 5.1 shows the strategy utilized for functionalization of Si(111), using a two-step chlorination/alkylation method followed by Cu(I)-catalyzed click chemistry. The acetylene passivation leads to a high coverage of atop sites on an unreconstructed Si(111) surface ($97 \pm 5\%$), which resists native oxidation of the surface.^{39,40} Another advantage is the ability to use the terminal alkyne to attach a variety of molecules via click chemistry.

The starting surfaces used in these experiments were single crystal, polished Si(111) wafers that were 500 to 550 μm thick, phosphorus-doped (n-type), with 0.005 to 0.02 $\Omega\text{-cm}$ resistivity, and a miscut angle of 3° - 4° (Montco Silicon Technologies; Spring City, PA). Prior to use, the Si wafers (1 cm \times 1 cm) were cleaned by successive sonications in acetone, methanol, and isopropanol. Substrates were then rinsed with Millipore (18 M Ω) water and then placed into basic piranha solution (5:1:1 = $\text{H}_2\text{O}:\text{H}_2\text{O}_2$:



Scheme 5.1. Strategy for the functionalization of Si(111).

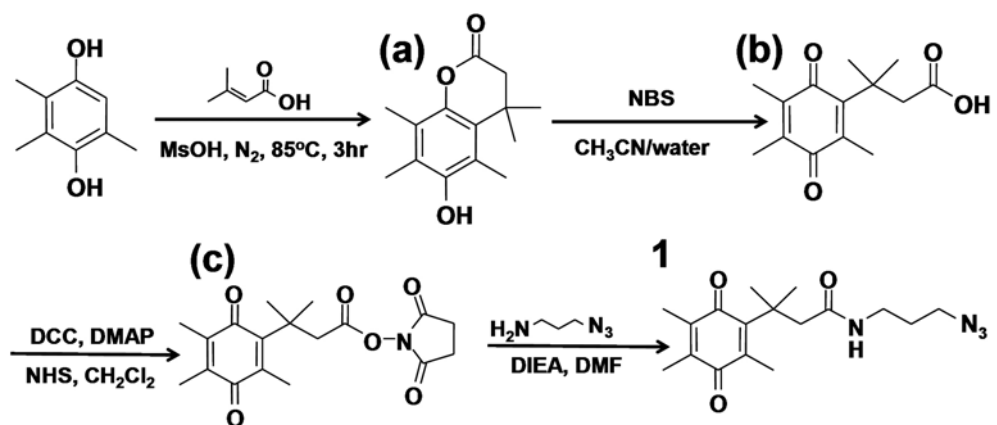
NH₄OH *warning: caustic!*) at 80 °C for 5 min. The samples were removed from piranha solution, rinsed with copious amounts of Millipore water and dried under streaming N₂(g). The samples were immediately placed in degassed NH₄F(aq) solution for 15 min. The samples were subsequently removed from the NH₄F(aq), rinsed copiously with water, dried under streaming N₂(g), and immediately loaded into a glove box.

Chlorination of the Si(111) surfaces (Scheme 5.1, Step 1) was carried out in a N₂(g)-purged glove box, according to published methods.³³⁻⁴⁰ A saturated solution of PCl₅ in chlorobenzene was prepared and heated for 1 h before use to ensure complete dissolution of the PCl₅. The Si substrate was added with a grain of benzoyl peroxide to this solution and heated to 90 °C for 50 min. Subsequently, the samples were rinsed with anhydrous THF several times and immediately used for the acetylenylation step.

Acetylenylation of the chlorinated Si(111) surfaces (Scheme 5.1, Step 2) was performed inside the N₂(g)-purged glove box. The chlorinated wafers were immersed in a sodium acetylide (18 wt% in xylenes/light mineral oil) suspension and heated to 130 °C for 5 h.⁴³ After reaction, the samples were removed from solution, rinsed copiously with anhydrous THF, and then rinsed with anhydrous methanol. The samples were then immersed into a fresh volume of anhydrous methanol, removed from the glove box into air, sonicated for 10 min, and then dried in a stream of N₂(g).

5.2.3 Synthesis of Electroactive Benzoquinone 1

Scheme 5.2 describes the synthetic procedure for making the electroactive benzoquinone **1** used for all surface click reactions.⁵⁷ A 2,3,5-trimethylhydroquinone was treated with dimethylacrylic acid to give a lactone (**a**) by a Friedel-Crafts type



Scheme 5.2. Synthesis of electroactive benzoquinone **1**.

addition reaction. The quinone acid (**b**) was prepared by oxidation of the resulting lactone (**a**) with aqueous N-bromosuccinimide (NBS). The acid was activated with an N-hydroxysuccinimidyl (NHS) group to give (**c**), which was then subjected to 3-azidopropylamine to afford **1**.

6-Hydroxy-4,4,5,7,8-peptamethyl-chroman-2-one (a). 2,3,5-Trimethylhydroquinone (2 g, 13.1 mmol) was mixed with 3,3-dimethylacrylic acid (1.45 g, 14.5 mmol) and methanesulfonic acid (10 mL). The mixture was stirred at 85 °C under nitrogen for 3 h and then cooled to room temperature. To the mixture, 100 g of ice was added with stirring. The precipitate was extracted with ethyl acetate (4 × 50 mL). The combined organic layer was washed with saturated NaHCO₃ (2 × 50 mL) and water (2 × 50 mL), and dried over MgSO₄. After filtration and evaporation, an obtained residue was recrystallized from hexane and ethyl acetate (2:1, v/v) to give 2.6 g (84%) of the desired product as a white solid. ¹H NMR 300 MHz (CDCl₃) δ 4.69 (s, 1H), 2.56 (s, 2H), 2.37 (s, 3H), 2.23 (s, 3H), 2.9 (s, 3H), 1.46 (s, 6H).

3-Methyl-3-(2,4,5-trimethyl-3,6-dioxocyclohexa-1,4-dienyl)butanoic acid (b). To a solution of the lactone **a** (1.58 g, 6.74 mmol) in a mixture of acetonitrile (15 mL) and water (3 mL) was added N-bromosuccinimide (1.26 g, 7.08 mmol) in portions with stirring at room temperature. After 30 min, the organic solvents were evaporated under reduced pressure, and the remaining solution was extracted with CH₂Cl₂ (2 × 30 mL). The combined organic layer was dried over MgSO₄, and reduced solvent to give 1.65 g (98%) of a yellow oily product, which was used without further purification. ¹H NMR 300 MHz (CDCl₃) δ 3.04 (s, 2H), 2.15 (s, 3H), 1.96 (m, 3H), 1.94 (m, 3H), 1.45 (s, 6H).

3-Methyl-3-(2,4,5-trimethyl-3,6-dioxocyclohexa-1,4-dienyl)butanoic acid, N-hydroxysuccinimidyl ester (c). To a solution of acid **b** (326 mg, 1.30 mmol) and N-hydroxysuccinimide (152 mg, 1.32 mmol) in CH₂Cl₂ (15 mL), was added 1,3-dicyclohexylcarbodiimide (DCC, 270 mg, 1.31 mmol) portionwise, followed by a catalytic amount of *N,N*-dimethylaminopyridine (DMAP). The reaction mixture was stirred for 1 h. The white precipitate was filtered and the filtrate was concentrated. The residue was redissolved in cold ethyl acetate (5 mL) and insoluble impurities were filtered. Solvent was removed to give 419 mg (93%) of a yellow foamy solid product. ¹H NMR 300 MHz (CDCl₃) δ 3.27 (s, 2H), 2.77 (s, 4H), 2.15 (s, 3H), 1.94 (s, 6H), 1.51 (s, 6H).

N-(3-azidopropyl)-3-methyl-3-(2,4,5-trimethyl-3,6-dioxocyclohexa-1,4-dienyl) butanamide (1). To a solution of **c** (443 mg, 1.28 mmol) in DMF (5 mL) was added diisopropylethylamine (DIEA, 523 μL, 3.06 mmol), followed by 3-azidopropylamine (153 mg, 1.53 mmol). The reaction mixture was stirred overnight at 50 °C, diluted with ethyl acetate (30 mL), washed with NH₄Cl and brine, and dried over MgSO₄. Solvent was reduced and the residue was purified by silica gel chromatography (hex/EtOAc, 2:1) to give 370 mg (87%) of product as a yellow solid. ¹H NMR 300 MHz (CDCl₃) δ 3.30 (t, J = 6.6, 2H), 3.23 (q, J = 6.6, 2H), 2.81 (s, 2H), 2.12 (s, 3H), 1.96 (m, 3H), 1.94 (m, 3H), 1.70 (quint, J = 6.6, 2H), 1.41 (s, 6H). Mass (ES) m/z 333.0 ([M + H]⁺).

5.2.4 Click Reaction to Attach **1** onto Acetylene-Terminated Si(111)

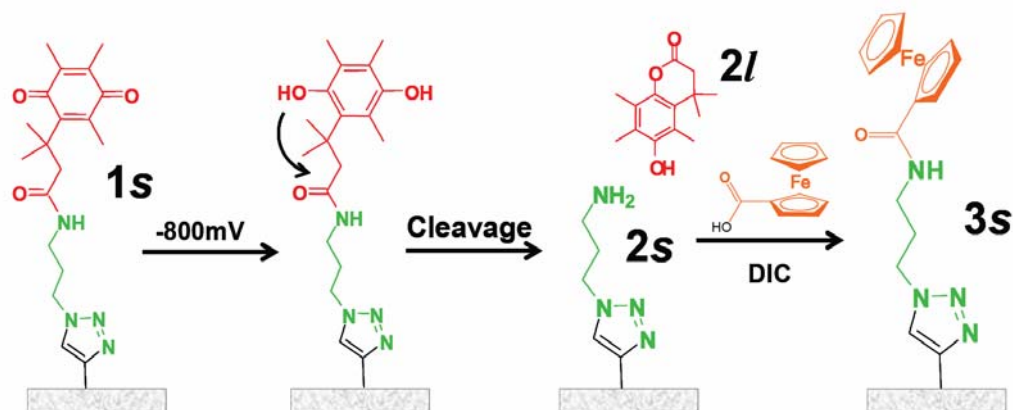
The click reaction of acetylene-terminated Si(111) (Scheme 5.1, Step 3) with **1**

(Scheme 5.2) was carried out in anhydrous DMF. Relative to the azide, 20 mol% sodium ascorbate was added, followed by 10 mol% of $\text{CuSO}_4 \cdot 5\text{H}_2\text{O}$, and a 10 mM azide solution of **1** in DMF. The reaction was run for 12 h in the glove box. After the reaction, the surface was sonicated in DMF for 3×5 min and then rinsed with methanol and blow dried under $\text{N}_2(\text{g})$.

5.2.5 Electrochemical Activation to Attach Ferrocene Carboxylic Acid and Biotin

1 was attached to acetylene-terminated Si(111) using the Cu(I)-catalyzed click reaction (Scheme 5.1, Step 3), to form **1s** (Scheme 5.3). Reductive electrochemistry (-800 mV referenced to Ag/AgCl) was performed to convert the modified benzoquinone to hydroquinone in degassed DPBS (pH 7.4). The hydroquinone then underwent an intramolecular cyclization reaction, leaving a free amine on the surface (**2s**) and releasing a lactone species (**2l**). This amine terminus allows for a variety of subsequent reactions, including amide coupling chemistry, which is commonly utilized to attach biomolecules to surfaces. We first illustrated the use of this electrochemical reduction process to attach ferrocene carboxylic acid to the surface, to form **3s**, via amide coupling chemistry. Ferrocene carboxylic acid (0.02 M) and *N,N'*-diisopropylcarbodiimide (DIC) (0.13 M) in DMF were added to the free amine surface. The amide coupling reaction was run overnight covered in an N_2 -purged glove box. The surface was then sonicated three times in DMF, then MeOH, and then blown dry.

Similarly, biotin (0.02 M) and DIC (0.13 M) in DMF were added to the free amine surface **2s**. The amide coupling reaction was run overnight in an N_2 -purged glove box at 50 °C. The surface was then sonicated three times in DMF, then MeOH, and blow dried. Subsequently, the Nanogold streptavidin (10 pM in 0.05% Tween20/DPBS)



Scheme 5.3. The chemical and electrochemical steps involved in non-oxidatively activating Si(111) surfaces. The molecules or molecular components are colored to highlight their different functions. **1s** represents the surface-bound benzoquinone that resulted from the click reaction of **1** to the acetylene-modified Si(111) surface (reacted acetylene group drawn in black). Upon reduction at -800 mV (vs. Ag/AgCl) of the benzoquinone to the hydroquinone, an intramolecular cyclization reaction ensues to produce **2l** (red lactone leaving group) and **2s** (the green triazole ring with an amine terminus). This represents the activated surface. The ferrocene carboxylic acid (orange), a second electrochemically active molecule, is then coupled to the Si(111) surface.

was introduced for 15 min. The surface was sonicated in 0.05% Tween20/DPBS for 25 min and then water for 5 min. The gold particles were then amplified with gold enhancement reagents for 10 min and then sonicated in water for 5 min.

5.3 SURFACE CHARACTERIZATION

5.3.1 X-ray Photoelectron Spectroscopy

X-ray photoelectron spectroscopy (XPS) was utilized to characterize many of the steps of both Schemes 5.1 and 5.3. All XPS measurements were performed in an ultra-high vacuum chamber of an M-probe surface spectrometer that has been previously described.⁵⁹ All measurements were taken on the center of the sample at room temperature. Monochromatic Al K α X-rays (1486.6 eV) were incident at 35° from the sample surface and were used to excite electrons from samples. The emitted electrons were collected by a hemispherical analyzer at a take-off angle of 35° from the plane of the sample surface.

ESCA-2000 software was employed to collect and analyze the data. To get an overview of the species present in the sample, survey scans were run from 0 to 1000 binding eV (BeV). The Si 2p (97-106 BeV), Cl 2p (196-206 BeV), C 1s (282-292 BeV), N 1s (393-407 BeV), Fe 2p (695-745 BeV), and Au 4f (77-97 BeV) regions were investigated in detail.

5.3.2 Contact Angle Goniometry

The sessile contact angle of water on the functionalized Si(111) surface was utilized as a measurement of the fidelity of the monolayer for all surfaces of Schemes 5.1 and 5.3 except H- and Cl-terminated Si(111). Contact angle measurements were

obtained with an NRL C.A. Goniometer Model #100-00 (Rame-Hart) at room temperature. Contact angles, θ , were measured from sessile drops by lowering a 1 μL drop from a syringe needle onto the surface. This was repeated three times and averaged to obtain the θ for the surface.

5.3.3 Electrochemical Characterization of Surface Coverages

Reductive electrochemistry was performed on **1s** in a custom-made cell using a VMP Multi-Potentiostat (Princeton Applied Research, Oak Ridge, TN) (Figure 5.3). Dulbecco's Phosphate Buffered Saline (DPBS) was used as the electrolyte, with silicon as a working electrode, a Pt coil as a counter electrode, and an Ag/AgCl reference electrode. Cyclic voltammetry was carried out at a rate of 100 mV/s. Molecular coverage was obtained by integrating the cathodic peak of the first scan in which all the modified benzoquinone was reduced to hydroquinone.

5.3.4 Fourier-Transform Infrared Spectroscopy

The H- and H-C \equiv C-terminated Si(111) surfaces were characterized by Attenuated Total Reflection Fourier Transform Infrared Spectroscopy (ATR-FTIR). The Si(111) surfaces were prepared from single-crystal, polished Si(111), miscut 3°-4°, boron-doped (p-type), 500 to 550 μm thick, and with 4 to 20 $\Omega\text{-cm}$ resistivity (Addison Engineering; San Jose, CA). Samples were cut into (2 cm \times 2 cm) pieces. Samples underwent the acetylenylation and click reactions as described above. Samples were mounted on a Germanium ATR crystal (GATR, Harrick Scientific Products) for a grazing angle of 65°. The sample was placed in a Vertex 70 FT-IR spectrometer (Bruker

Optics) for measurements. In an air-purged sample chamber, 512 or 1024 scans were taken, with background scans of air subtracted from the spectra. Spectra were fitted with a linear baseline prior to analysis.

5.4 RESULTS

5.4.1 XPS Survey Scans and Contact Angle Measurements

XPS survey scans revealed the progression of the acetylenylation and click chemistry steps. For a freshly prepared, H-terminated Si(111) surface (H-[Si(111)]), Si 2p and Si 2s peaks were observed, at 100 BeV and 150 BeV, respectively. Additional small C 1s and O 1s peaks, corresponding to adventitiously adsorbed carbon and oxygen on the surface, were also detected. After chlorination of H-[Si(111)] by PCl_5 , two new peaks at 200 BeV and 270 BeV appeared in the XPS spectrum, representing the Cl 2p and Cl 2s electrons, respectively. Upon a treatment with sodium acetylide, the chlorine peaks disappeared completely and a pronounced C 1s appeared at 285 BeV, verifying that the acetylene-terminated Si(111) surface (H-C \equiv C-[Si(111)]) has been generated. Other adsorbed carbon can contribute to the C 1s peak intensity for this scan. After the click reaction with electroactive quinone **1**, a new N 1s peak appears at 400 BeV.

Sessile contact angles were also quantified for the various surface functionalization steps described in Schemes 5.1 and 5.3, and those values are listed in Table 5.1.

5.4.2 High-Resolution XPS Measurements

High-resolution XPS measurements were utilized to quantitate the chemical steps of Schemes 5.1 and 5.3. In particular, the Si 2p region was used to monitor the growth

Table 5.1. Measured contact angles for various Si(111) surfaces.

Surfaces	Contact Angle (°)
H-C≡C-[Si(111)]	77 ± 2
1s	68 ± 2
2s	60 ± 2
3s	59 ± 2

of silicon oxides as a function of exposure time to air (Figure 5.1) and as a function of the chemical and electrochemical steps of Scheme 5.3 (Figure 5.2A) in two sets of experiments. For both measurements, a Shirley baseline was applied to each spectrum before the peaks were fitted. Peak line shapes for bulk Si $2p_{3/2}$ and $2p_{1/2}$ were fitted to Voigt functions fixed at 95% Gaussian and 5% Lorentzian, with a 15% asymmetry. The Si $2p_{1/2}$ and $2p_{3/2}$ peaks were fitted with the two peaks held 0.6 BeV apart, the full width at half maximum (FWHM) was fixed at 1, and the integrated area ratio of the $2p_{1/2}/2p_{3/2}$ peaks was fixed at 0.51, as has been previously described.^{33–35,42} The broad peak between 100 and 104 BeV was assigned as Si^+ to Si^{4+} oxides and was fitted to a third peak. The positions of the three peaks and the width of the third peak were optimized to obtain the best fit to the experimental spectrum. For very thin oxide layers, the oxide coverage was calculated from the $\text{SiO}_x:\text{Si}$ 2p peak area ratio. This was determined by dividing the area under the third peak by the total area of the Si $2p_{3/2}$ and $2p_{1/2}$ peaks.³⁵ The $\text{SiO}_x:\text{Si}$ 2p peak area ratio was then divided by a normalization constant of 0.21 for Si(111) to estimate the fraction of surface atoms that was oxidized.^{33–35}

We estimated that there were approximately 0.25 equivalent monolayers of SiO_x on the acetylene-terminated Si(111) surface after 6 days' exposure to air (Figure 5.1). This is consistent with other results that have shown stability toward oxidation for as long as 60 days in air.⁴³ Following the formation of **1s** and the reduction of **1s** to **2s** at -800 mV (Scheme 5.3) in aqueous electrolyte, the amount of SiO_x was calculated to be 0.29 and 0.34 equivalent monolayers, respectively.

The $\text{H-C}\equiv\text{C}[\text{Si}(111)]$ surface was also characterized using high-resolution C 1s XPS (Figure 5.2B). The resulting spectrum was deconvoluted and fitted to three peaks, the silicon-bonded carbon at 283.8 BeV, the carbon-bonded carbon at 284.9 BeV,

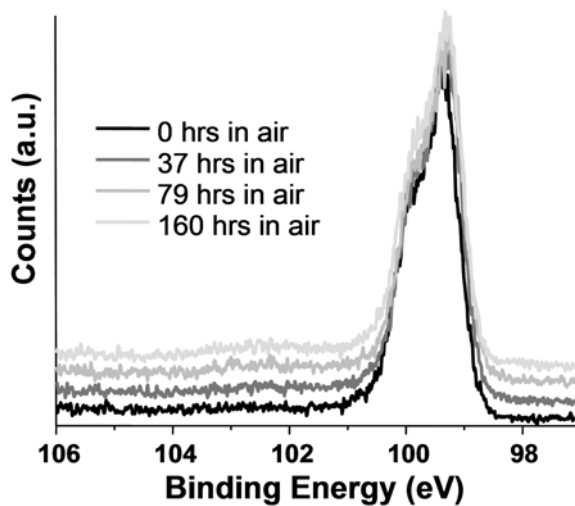


Figure 5.1. XPS data of H-C≡C-[Si(111)], collected in the Si 2p region, and taken after exposure to air for up to 160 h. The peaks for SiO_x species should appear between 100 and 104 BeV. The amount of oxidation of the Si(111) can be estimated from this data to be about 0.25 equivalent monolayers. The Si 2p features are normalized to the same height for all three scans. The 37, 79, 160 h scans are shown offset from the 0 h scan to reveal the spectral detail.

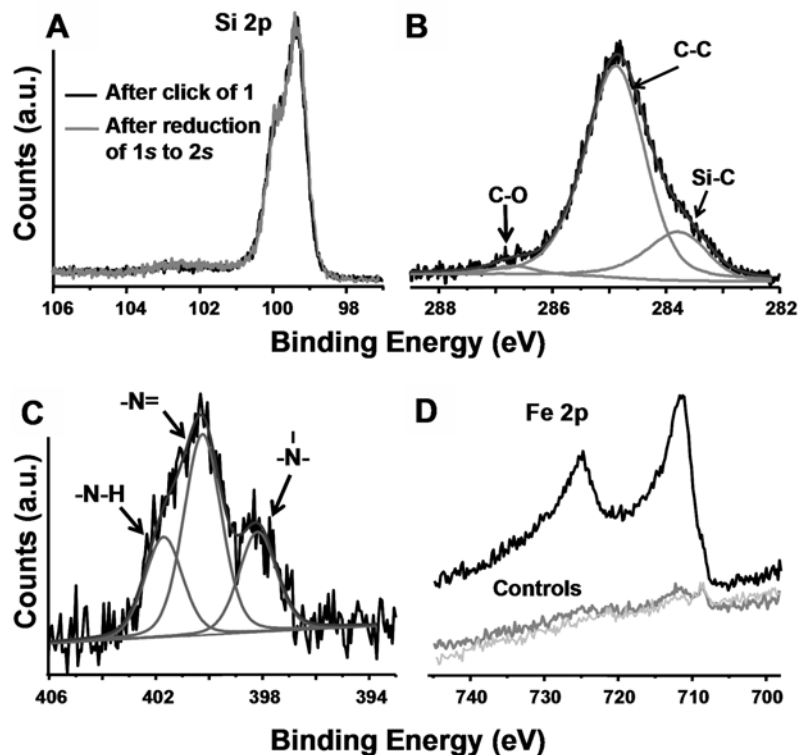


Figure 5.2. High-resolution XPS spectra of H-C≡C-[Si(111)], and of that surface following the click reaction to form **1s** and the reduction of **1s** to **2s**. **(A)** Si 2p region revealing the near absence of oxide growth during the Cu(I)-catalyzed click reaction, and during the reductive transformation of **1s** to **2s**. **(B)** Scan of the C 1s region of H-C≡C-[Si(111)]. The Si-C peak is unique to H-C≡C-[Si(111)] surfaces. The C-C peak contains contributions from the C≡C bond and adventitious carbon from the environment. The C-O peak present also arises from adventitious hydrocarbons. **(C)** Scan of the N 1s region of **1s**, validating the click formation of **1s**. The area ratio of the three peaks is 1:2:1, respectively. **(D)** Scan of the Fe 2p region showing the formation of **3s** via the amide coupling of ferrocene carboxylic acid to **2s**. The control plots are of **1s** (dark grey) and the H-C≡C-[Si(111)] surface (light grey) after exposure to ferrocene carboxylic acid under the same conditions.

and the oxygen-bonded carbon at 286.8 BeV. As developed by Nemanick,^{41,42} peaks were fitted to Voigt functions having 70% Gaussian and 30% Lorentzian line shapes. The peak center-to-center distances were fixed at 1.1 BeV between the Si-C and C-C peaks, and at 2.9 BeV between the Si-C and O-C peaks. To calculate the surface coverage of the acetylene, the integrated area under the silicon-bonded carbon peak was ratioed to the total integrated area of the Si 2p_{3/2} and 2p_{1/2} peaks and normalized with respect to scan time. The ratio calculated was referenced to a methyl-terminated Si(111) surface that was scanned under the same conditions. The effective coverage of acetylene on the Si surface was $97 \pm 5 \%$, consistent with other measurements of such surfaces.⁴³ The statistical uncertainty in this number is largely determined by the signal-to-noise ratio of the XPS data (~30:1).

The high-resolution N 1s spectrum of **1s** illustrates the attachment of the benzoquinone (**1**) via click chemistry (Figure 5.2C). There is no peak at 405 BeV, signifying the absence of free azide. This result indicates that the azide-modified electroactive benzoquinone is not just freely adsorbed but covalently bonded to the surface.⁵² The N 1s spectrum was deconvoluted and fitted to three peaks, each composed of 80% Gaussian and 20% Lorentzian line shapes.⁶⁰ The three peaks correspond to the amide nitrogen at 401.7 BeV, the doubly bonded nitrogen atoms (in the 1,2,3-triazole ring) at 400.3 BeV, and the singly bonded nitrogen (in the 1,2,3-triazole ring) at 398.2 BeV, respectively. The ratio of peak areas was found to be 1:2:1, consistent with the structure of **1s**. After electrochemical cleavage to **2s**, the N 1s region remained unchanged.

Figure 5.2D is a high-resolution scan of the Fe 2p region that demonstrates the attachment of ferrocene carboxylic acid onto **2s** to form **3s**. The Fe 2p_{3/2} and 2p_{1/2} peaks

occur at 711.3 and 724.8 BeV, respectively. It is difficult to quantify the amount of iron from such data because the peak shape is highly asymmetric and hard to deconvolute with a single Gaussian/Lorentzian function due to the strong multiplet splitting.⁶⁰ However, as discussed below, the surface coverage of **3s** can be estimated from cyclic voltammetry measurements. Figure 5.2D also shows two control experiments. Although a trace amount of ferrocene residue was detected on the controls, this measurement does confirm that the large majority of ferrocene is the result of the covalent bond formation between carboxylic acid of the ferrocene and the free amine of **2s**.

5.4.3 Electrochemical Measurements

Figure 5.3A depicts the cyclic voltammogram (CV) for **1s**. The prominent cathodic peak in the first scan confirms the presence of electroactive benzoquinone and, therefore, that the click reaction proceeded. Molecular coverage was obtained by integrating the cathodic peak of the first scan, where all the modified benzoquinone was reduced to hydroquinone. Complete conversion of **1s** to **2s** accompanied by the release of **2I** (Scheme 5.3) was achieved at potentials below -0.9 V. Consecutive CV scans demonstrated that no detectable benzoquinone remained. For the determination of coverage, the area under the cathodic peak was obtained after subtracting the non-Faradaic current. This area was converted to the number of molecules by a stoichiometric ratio of 2 electrons to 1 electroactive molecule. Then, the number of molecules was divided by the electrode surface area and then normalized to the Si atop atom surface density (7.8×10^{14} /cm² for Si(111)).¹⁷ The coverage calculated for **1s** on the H-C \equiv C-[Si(111)] was 6.7 ± 0.3 %.

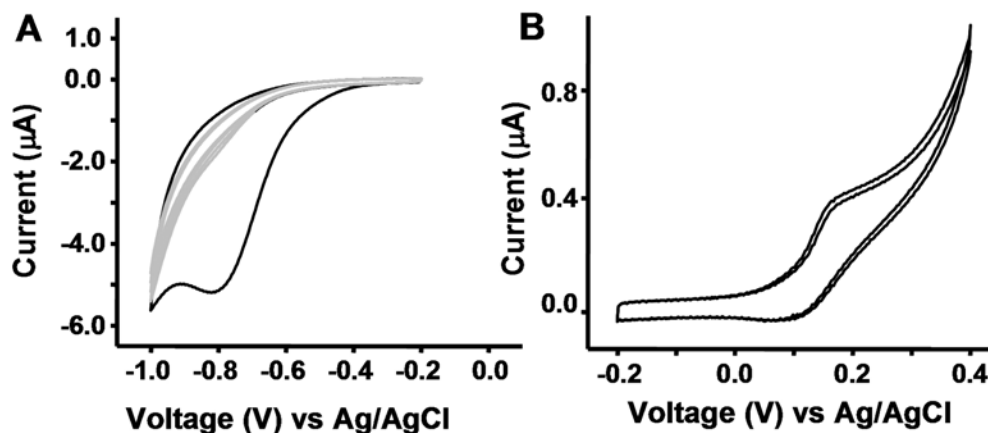


Figure 5.3. Cyclic voltammograms (CVs) for **1s** and **3s**. **(A)** The electrochemical activation of **1s** to **2s**. The black trace is of the first scan, and the grey traces are of two subsequent scans, indicating nearly complete conversion of benzoquinone to hydroquinone during the first scan. **(B)** The reversible oxidation of **3s**. Two subsequent scans are shown. CVs were performed at a rate of 100 mV/s with voltages relative to Ag/AgCl.

The amine terminus presented by **2s** provides a handle for subsequent reaction, including amide coupling chemistry, which is commonly utilized to attach biomolecules to surfaces. An exemplary surface is **3s**, the product of the amide coupling of ferrocene carboxylic acid with **2s**. The CVs of **3s** (Figure 5.3B) display reversible $\text{Fc}^{0/+}$ redox behavior, as expected for ferrocene oxidation. The peak spacing confirms that ferrocene is covalently attached (but not adsorbed) onto the surface. The coverage was calculated by integrating the anodic peak after subtracting the non-Faradaic current. The number of molecules was divided by the electrode surface area and normalized to Si atom surface density which is $7.8 \times 10^{14}/\text{cm}^2$ for Si(111).¹⁷ The coverage calculated for **3s** was 0.5%. We do not fully understand the low coverage of ferrocene molecules. A likely possibility is that the time and/or temperature conditions for the coupling reaction were not optimal. It is also possible that degradation of the surface by oxidative potential treatments might also reduce the coverage of ferrocene.

5.5 DISCUSSION

The coverage values for H-C \equiv C-[Si(111)], surface **1s**, and surface **3s** are summarized in Table 5.2, calculated with respect to all atop sites on an unreconstructed Si(111) surface.

The 97% coverage of the H-C \equiv C-[Si(111)] surface is consistent with the Si 2p XPS in Figure 5.1 (and other studies⁴³) that indicated little surface-bound SiO_x. The acetylene carbons are *sp*-hybridized, implying a perpendicular attachment to the Si(111) surface. The atomic radius for C is smaller than that for Si (0.70 Å versus 1.10 Å), and there is a 3.8-Å spacing between atop sites on Si(111). These values support the notion

Table 5.2. The molecular surface coverages for various Si(111) surfaces, as measured by XPS or electrochemistry (EC).

Surfaces	Coverage (%)
H-C≡C-[Si(111)]	97 ± 5 (XPS)
1s – benzoquinone	6.7 ± 0.3 (EC)
3s – ferrocene	0.5 (EC)

that a 100% passivation of Si(111) surfaces can be achieved using the approach we described here.

Additional support for 100% acetylenylation of Si(111) comes from the ATR-FTIR measurements of H-[Si(111)] and H-C≡C-[Si(111)] (Figure 5.4; black and grey traces, respectively). Whereas XPS allows analysis of the elemental composition of surfaces, infrared spectroscopy (IR) gives information about the types of chemical functionality on a surface. The spectra shown in Figure 5.4 are expanded to highlight the region containing the signature Si-H (2083 cm^{-1}) stretching frequency that is observed for the H-[Si(111)]. The Si-H stretch is strong and sharp, indicating that the surface sites are passivated with one hydrogen atom per atop site. This is expected for a H-[Si(111)] freshly prepared by an $\text{NH}_4\text{F}(\text{aq})$ etch.⁶¹ For H-C≡C-[Si(111)], the 2083 cm^{-1} vibration has quantitatively disappeared, again consistent with 100% acetylenylation and with other work.⁴³ A weak C≡C stretch might be expected in this region (2120 to 2175 cm^{-1}),^{43,49} although we have not observed it. When H-[Si(111)] is ethylated through a similar chlorination/alkylation procedure, the coverage of ethyl groups on the atop sites of the Si(111) surface is reduced by steric interactions to approximately 80%.⁴⁰ Following the Grignard alkylation of Si(111), no Cl is detected on the surface,³³ and FTIR data indicates that the remaining Si(111) atop sites are hydrogenated.⁶² For the ethylated surface, the 2083 cm^{-1} feature is broadened, shifted (to 2070 cm^{-1}) and reduced in intensity to 14% of that observed for the H-[Si(111)] surface.⁶²

The coverage of the electroactive benzoquinone **1** on Si(111) to form **1s** was calculated to be ~7% of all available Si(111) atop sites. We previously reported on electrochemically activating Si(111) and Si(100) surfaces through the use of protected

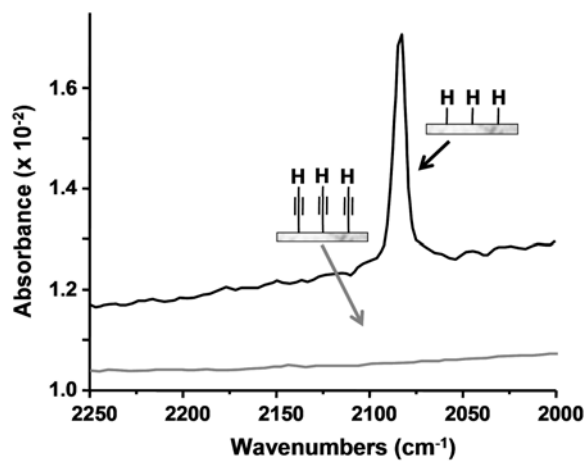


Figure 5.4. ATR-FTIR characterization of a H-[Si(111)] and H-C≡C-[Si(111)], in the region of the 2083 cm⁻¹ Si-H mode.

hydroquinones that were attached to H-terminated Si surfaces via UV activation.¹⁷ For those molecules, coverages of up to 23% were achievable on Si(111), although bulkier protection groups on the hydroquinone led to slightly reduced surface coverages, implying steric interactions played at least some role in limiting coverage. It is likely that steric interactions play a dominating role in determining the efficiency of the click reaction to form **1s**. While the acetylene footprint may be approximated by the van der Waals radius of the carbon atom, the 1,2,3-triazole ring formed upon the click reaction will obviously be much larger. In fact, it is possible that the click chemistry is only effective at the step edges of the Si(111) surface. We have extensively characterized various Si(111) surfaces that have been alkylated using the two-step chlorination/alkylation chemistry using high-resolution Scanning Tunneling Microscopy (STM). For both methylated^{34,39} and ethylated⁴⁰ Si(111), we find that about 10% of the Si surface atoms lie at step edges. This arises from etch pits that are apparently formed during the chlorination step, implying that the H-C≡C-[Si(111)] surface likely shares a similar morphology. In that case, acetylene groups located at step edges would not have the steric constraints that would limit the formation of the triazole ring. It is interesting that the 7% coverage of **2s** is similar to the number of Si atop sites that would reside at step edges. We are currently investigating the H-C≡C-[Si(111)] and **1s** surfaces using high-resolution STM to test this hypothesis.

We observed minimal oxide growth on an acetylenylated surface even after 6 days' exposure to air, indicating nearly 100% passivation of the surface (Figure 5.1). Following the formation of **1s** and electrochemical reduction of **1s** to **2s** to reveal the free amine, the amount of SiO_x was slightly increased to 0.29 and 0.34 equivalent monolayers, respectively. The oxidation growth observed was due to the click chemistry

on acetylenylated surfaces that were minimally exposed to air during cleaning and preparation for reaction, and the electrochemistry which was carried out in an ambient (and aqueous) environment. It is notable that the limited oxide growth on the silicon even after all surface modifications afforded well-behaved electrodes.

There have been several reported examples of click reactions on metal surfaces, although relatively few papers have attempted to report quantitative coverage values. Chidsey's group⁵¹⁻⁵³ has reported on coverages of up to 55% of ferrocene molecules clicked onto $\text{N}_3\text{-(CH}_2\text{)}_n\text{-S-[Au]}$ SAMs. On gold, each organic group has approximately twice the area available to it, as compared with the area available to each acetylene group on Si(111) [$21.4 \text{ \AA}^2/\text{molecule}$ for gold and $12.8 \text{ \AA}^2/\text{molecule}$ for Si(111)].^{17,63,64} However, even for the much more loosely packed SAM, steric interactions were attributed as the reason for the incomplete (55%) yield of the click reaction.

The stated goal of this work was to develop a general strategy for electrochemically directing the biofunctionalization of Si(111) surfaces without oxidizing the underlying Si(111). To this end, we demonstrated the electrochemical activation and subsequent attachment of the model biomolecule, biotin, using a modification of the chemistry described in Scheme 5.3 (see Experimental Methods). To detect surface-bound biotin, we utilized Au nanoparticle-labeled streptavidin (strept-Au) and followed through with electroless amplification of the Au to produce particles that were imaged using Scanning Electron Microscopy (SEM). Representative data from this experiment, shown in Figure 5.5, indicate that the selectivity for attachment of strept-Au onto **2s** is about 100-fold greater than on two control surfaces, $\text{H-C}\equiv\text{C-[Si(111)]}$ and **1s**, both of which were also treated with biotin and exposed to strept-Au.

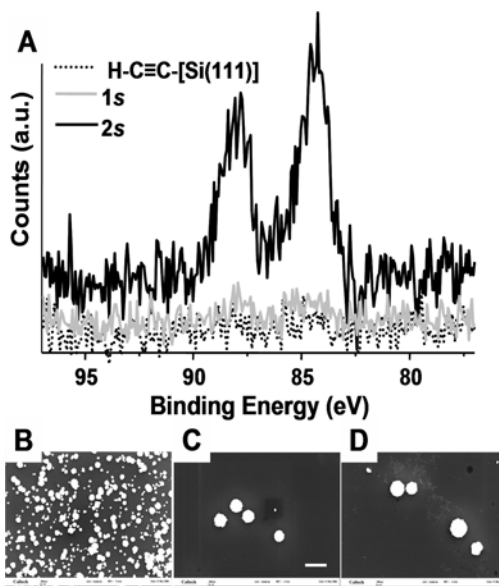


Figure 5.5. Demonstration of bioattachment to acetylenylated Si(111) through reductive formation of **2s** followed by the amide coupling of biotin. **(A)** XPS of the biotinylated Si(111) surface following exposure to strept-Au, but prior to the electroless Au amplification. The Au 4f region is comprised of two spin-orbit coupled peaks: Au 4f_{7/2} (~84 BeV) and Au 4f_{5/2} (~88 BeV). The dotted trace is from H-C≡C-[Si(111)], and the grey trace is from **1s**, each exposed to biotin and strept-Au as controls. The three SEM images **(B, C, D)** are of the activated and biofunctionalized surface, plus two controls. All images were taken following the electroless amplification step. The scale bar is 1 μm . **(B)** **2s**, incubated with biotin, and exposed to strept-Au. **(C)** H-C≡C-[Si(111)] incubated with biotin, and exposed to strept-Au. **(D)** **1s** incubated with biotin, and exposed to strept-Au. There are at least 500 Au nucleation sites on B, 5 on C, and 7 on D.

5.6 CONCLUSIONS

Acetylenylation of the Si(111) surface via the two-step chlorination/alkylation procedure was combined with click chemistry to provide a non-oxidative approach for adding chemical functionality to a silicon surface. Si(111) surfaces can be nearly 100% passivated with acetylene groups. A specifically designed, electroactive benzoquinone molecule has been immobilized to the H-C≡C-[Si(111)] surface. A 7% coverage of the benzoquinone was found, suggesting that the click reaction may have occurred at step edges on the H-C≡C-[Si(111)] surface. The attachment of an electroactive benzoquinone was highly selective and was accomplished with only a minimal amount of oxidation of the underlying Si(111). The electroactive benzoquinone was reduced and cleaved from the surface to produce an amine terminus. In separate experiments, ferrocene carboxylic acid and biotin were selectively and covalently immobilized to the electrochemically activated surface.

We believe this approach can be employed as a general platform to prepare functional surfaces for various applications and can be extended toward the selective biopassivation of arrays of various types of nanomechanical and/or nanoelectronic sensor devices.

5.7 ACKNOWLEDGEMENTS

This work was completed in collaboration with Rosemary D. Rohde, Woon-Seok Yeo, and Ryan C. Bailey. The XPS measurements were carried out at the Molecular Materials Research Center of the Beckman Institute at Caltech. We thank Professor Nate Lewis, Dr. Bruce Brunshwig, Dr. Pat Hurley, and Dr. Joseph Nemanick for kind advice and help regarding the acetylenylation of Si(111).

5.8 REFERENCES

1. Zheng, G.; Patolsky, F.; Cui, Y.; Wang, W. U.; Lieber, C. M. *Nat. Biotechnol.* **2005**, *23*, 1294–1301.
2. Beckmann, N.; Zahnd, C.; Huber, F.; Bietsch, A.; Plückthun, A.; Lang, H.-P.; Güntherodt, H.-J.; Hegner, M.; Gerber, C. *Proc. Natl. Acad. Sci. USA* **2005**, *102*, 14587–14592.
3. Yue, M.; Lin, H.; Dedrick, D. E.; Satyanarayana, S.; Majumdar, A.; Bedekar, A. S.; Jenkins, J. W.; Sundaram, S. *J. Microelectromech. Syst.* **2004**, *13*, 290–299.
4. Reccius, C. H.; Mannion, J. T.; Cross, J. D.; Craighead, H. G. *Phys. Rev. Lett.* **2005**, *95*, 268101.
5. Stavis, S. M.; Edel, J. B.; Li, Y. G.; Samiee, K. T.; Luo, D.; Craighead, H. G. *J. Appl. Phys.* **2005**, *98*, 044903.
6. Fan, R.; Karnik, R.; Yue, M.; Li, D. Y.; Majumdar, A.; Yang, P. D. *Nano Lett.* **2005**, *5*, 1633–1637.
7. Karnik, R.; Castelino, K.; Fan, R.; Yang, P.; Majumdar, A. *Nano Lett.* **2005**, *5*, 1638–1642.
8. (a) Craighead, H. G.; James, C. D.; Turner, A. M. P. *Curr. Opin. Solid State Mater. Sci.* **2001**, *5*, 177–184. (b) Jung, D. R.; Kapur, R.; Adams, T.; Giuliano, K. A.; Mrksich, M.; Craighead, H. G.; Taylor, D. L. *Crit. Rev. Biotechnol.* **2001**, *21*, 111–154.
9. For example, (a) Woolley, A. T.; Hadley, D.; Landre, P.; deMello, A. J.; Mathies, R. A.; Northrup, M. A. *Anal. Chem.* **1996**, *68*, 4081–4086. (b) Pantoja, R.; Nagarah, J. M.; Starace, D. M.; Melosh, N. A.; Blunck, R.; Bezanilla, F.; Heath, J. R. *Biosens. Bioelectron.* **2004**, *20*, 509–517.

10. Piner, R. D.; Zhu, J.; Xu, F.; Hong, S.; Mirkin, C. A. *Science* **1999**, *283*, 661–663.
11. Lee, K.-B.; Park, S.-J.; Mirkin, C. A.; Smith, J. C.; Mrksich, M. *Science* **2003**, *295*, 1702–1705.
12. Jung, H.; Dalal, C. K.; Kuntz, S.; Shah, R.; Collier, C. P. *Nano Lett.* **2004**, *4*, 2171–2177.
13. Yousaf, M.; Mrksich, M. *J. Am. Chem. Soc.* **1999**, *121*, 4286–4287.
14. Hodneland, C. D.; Mrksich, M. *J. Am. Chem. Soc.* **2000**, *122*, 4235–4236.
15. Yeo, W.-S.; Yousaf, M. N.; Mrksich, M. *J. Am. Chem. Soc.* **2003**, *125*, 14994–14995.
16. Yeo, W.-S.; Mrksich, M. *Adv. Mater.* **2004**, *16*, 1352–1356.
17. Bunimovich, Y. L.; Ge, G.; Beverly, K. C.; Ries, R. S.; Hood, L.; Heath, J. R. *Langmuir* **2004**, *20*, 10630–10638.
18. Curreli, M.; Li, C.; Sun, Y.; Lei, B.; Gundersen, M. A.; Thompson, M. E.; Zhou, C. *J. Am. Chem. Soc.* **2005**, *127*, 6922–6923.
19. (a) Hu, K.; Fan, F.-R. F.; Bard, A. J.; Hillier, A. C. *J. Phys. Chem. B* **1997**, *101*, 8298–8303. (b) Yeganeh, M. S.; Dougal, S. M.; Pink, H. S. *Phys. Rev. Lett.* **1999**, *83*, 1179–1182.
20. (a) Israelachvili, J. *Intermolecular and Surface Forces* (London: Academic Press, 1985). (b) Lud, S. Q.; Nikolaidis, M. G.; Haase, I.; Fischer, M.; Bausch, A. R. *ChemPhysChem* **2006**, *7*, 379–384. (c) Neff, P. A.; Wunderlich, B. K.; Lud, S. Q.; Bausch, A. R. *Phys. Status Solidi A* **2006**, *203*, 3417–3423.
21. Buriak, J. M. *Chem. Rev.* **2002**, *102*, 1271–1308.

22. Yablonovitch, E.; Allara, D. L.; Chang, C. C.; Gmitter, T.; Bright, T. B. *Phys. Rev. Lett.* **1986**, *57*, 249–252.
23. Sung, M. M.; Kluth, G. J.; Yauw, O. W.; Maboudian, R. *Langmuir* **1997**, *13*, 6164–6168.
24. Sieval, A. B.; Demirel, A. L.; Nissink, J. W. M.; Linford, M. R.; van der Maas, J. H.; de Jeu, W. H.; Zuilhof, H.; Sudhölter, E. J. R. *Langmuir* **1998**, *14*, 1759–1768.
25. Effenberger, F.; Gotz, G.; Bidlingmaier, B.; Wezstein, M. *Angew. Chem. Int. Ed.* **1998**, *37*, 2462–2464.
26. Boukherroub, R.; Wayner, D. D. M. *J. Am. Chem. Soc.* **1999**, *121*, 11513–11515.
27. Linford, M. R.; Fender, P.; Eisenberger, P. M.; Chidsey, C. E. D. *J. Am. Chem. Soc.* **1995**, *117*, 3145–3155.
28. Cicero, R. L.; Linford, M. R.; Chidsey, C. E. D. *Langmuir* **2000**, *16*, 5688–5695.
29. Buriak, J. M.; Allen, M. J. *J. Am. Chem. Soc.* **1998**, *120*, 1339–1340.
30. Stewart, M. P.; Buriak, J. M. *J. Am. Chem. Soc.* **2001**, *123*, 7821–7830.
31. Boukherroub, R.; Morin, S.; Bensebaa, F.; Wayner, D. D. M. *Langmuir* **1999**, *15*, 3831–3835.
32. Zhang, L.; Li, L.; Chen, S.; Jiang, S. *Langmuir* **2002**, *18*, 5448–5456.
33. Webb, L. J.; Nemanick, E. J.; Biteen, J. S.; Knapp, D. W.; Michalak, D. J.; Traub, M. C.; Chan, A. S. Y.; Brunshwig, B. S.; Lewis, N. S. *J. Phys. Chem. B* **2005**, *109*, 3930–3937.
34. Yu, H. B.; Webb, L. J.; Ries, R. S.; Solares, S. D.; Goddard, W. A.; Heath, J. R.; Lewis, N. S. *J. Phys. Chem. B* **2005**, *109*, 671–674.
35. Webb, L. J.; Lewis, N. S. *J. Phys. Chem. B* **2003**, *107*, 5404–5412.

36. Bansal, A.; Li, X. L.; Yi, S. I.; Weinberg, W. H.; Lewis, N. S. *J. Phys. Chem. B* **2001**, *105*, 10266–10277.
37. Royea, W. J.; Juang, A.; Lewis, N. S. *Appl. Phys. Lett.* **2000**, *77*, 1988–1990.
38. Bansal, A.; Lewis, N. S. *J. Phys. Chem. B* **1998**, *102*, 4058–4060.
39. Solares, S. D.; Yu, H.; Webb, L. J.; Lewis, N. S.; Heath, J. R.; Goddard, W. A., III. *J. Am. Chem. Soc.* **2006**, *128*, 3850–3851.
40. Yu, H.; Webb, L. J.; Solares, S. D.; Cao, P.; Goddard, W. A., III; Heath, J. R.; Lewis, N. S. *J. Phys. Chem. B* **2006**, *110*, 23898–23903.
41. Nemanick, E. J. Chemical and electrical passivation of single crystal silicon surfaces through covalently bound organic monolayers. Ph.D. thesis: California Institute of Technology, 2005.
42. Nemanick, E. J.; Hurley, P. T.; Brunshwig, B. S.; Lewis, N. S. *J. Phys. Chem. B* **2006**, *110*, 14800–14808.
43. Hurley, P. T.; Nemanick, E. J.; Brunshwig, B. S.; Lewis, N. S. *J. Am. Chem. Soc.* **2006**, *128*, 9990–9991.
44. Kolb, H. C.; Finn, M. G., Sharpless, K. B. *Angew. Chem. Int. Ed.* **2001**, *40*, 2004–2021.
45. Bock, V. D.; Hiemstra, H.; van Maarseveen, J. H. *Eur. J. Org. Chem.* **2006**, 51–68.
46. Zhang, Y.; Luo, S.; Tang, Y.; Yu, L.; Hou, K.-Y.; Cheng, J. P.; Zeng, X.; Wang, P. G. *Anal. Chem.* **2006**, *78*, 2001–2008.
47. Lummerstorfer, T.; Hoffmann, H. *J. Phys. Chem. B* **2004**, *108*, 3963–3966.
48. Lee, J. K.; Chi, Y. S.; Choi, I. S. *Langmuir* **2004**, *20*, 3844–3847.

49. Li, H.; Cheng, F.; Duft, A. M.; Adronov, A. *J. Am. Chem. Soc.* **2005**, *127*, 14518–14524.
50. Zirbs, R.; Kienberger, F.; Hinterdorfer, P.; Binder, W. H. *Langmuir* **2005**, *21*, 8414–8421.
51. Collman, J. P.; Devaraj, N. K.; Chidsey, C. E. D. *Langmuir* **2004**, *20*, 1051–1053.
52. Collman, J. P.; Devaraj, N. K.; Eberspacher, T. P. A.; Chidsey, C. E. D. *Langmuir* **2006**, *22*, 2457–2464.
53. Devaraj, N. K.; Dinolfo, P. H.; Chidsey, C. E. D.; Collman, J. P. *J. Am. Chem. Soc.* **2006**, *128*, 1794–1795.
54. Devaraj, N. K.; Miller, G. P.; Ebina, W.; Kakaradov, B.; Collman, J. P.; Kool, E. T.; Chidsey, C. E. D. *J. Am. Chem. Soc.* **2005**, *127*, 8600–8601.
55. Giovanelli, D.; Lawrence, N. S.; Jiang, L.; Jones, T. G. J.; Compton, R. G. *Anal. Lett.* **2003**, *36*, 2941–2959.
56. Rousell, C.; Rohner, T. C.; Jensen, H.; Girault, H. H. *ChemPhysChem* **2003**, *4*, 200–206.
57. Zheng, A.; Shan, D.; Binghe, W. *J. Org. Chem.* **1999**, *64*, 156–161.
58. Yeo, W.-S.; Hodneland, C. D.; Mrksich, M. *ChemBioChem* **2001**, *2*, 590–593.
59. Haber, J. A.; Lewis, N. S. *J. Phys. Chem. B* **2002**, *106*, 3639–3656.
60. Babić-Samardžija, K.; Lupu, C.; Hackerman, N.; Barron, A. R.; Luttge, A. *Langmuir* **2005**, *21*, 12187–12196.
61. Dumas, P.; Chabal, Y. J.; Higashi, G. S. *Phys. Rev. Lett.* **1990**, *65*, 1124–1127.
62. Webb, L. J.; Rivillon, S.; Michalak, D. J.; Chabal, Y. J.; Lewis, N. S. *J. Phys. Chem. B* **2006**, *110*, 7349–7356.

63. Strong, L.; Whitesides, G. M. *Langmuir* **1988**, *4*, 546–558.
64. Chidsey, C. E. D.; Bertozzi, C. R.; Putvinski, T. M.; Muzsca, A. M. *J. Am. Chem. Soc.* **1990**, *112*, 4301–4306.